Izmir Institute of Technology

Department of Mechanical Engineering

ME 438 Assignment 4

Gamze Uyaroğlu

280203076

Fall 2025

Contents

Figures

AIRFOIL DESCRIPTION

In this study, the selected airfoil geometry is the NACA 4412, a widely used member of the four-digit NACA airfoil family. The NACA four-digit series airfoils are defined analytically by a set of four digits, each describing a specific geometric characteristic of the airfoil. These digits determine the maximum camber, the location of maximum camber, and the maximum thickness as percentages of the chord length. The nomenclature makes it possible to understand the airfoil geometry directly from its code.

For the NACA 4412 airfoil:

- First digit (4) → Represents the maximum camber, equal to 4% of the chord length.
- Second digit (4) → Indicates the location of the maximum camber, which is 40% of the chord length from the leading edge.
- Last two digits (12) → Define the maximum thickness, equal to 12% of the chord length.

Thus, the NACA 4412 is characterized by a relatively high camber and moderate thickness, making it suitable for low-speed aerodynamics applications requiring high lift generation, such as general aviation aircraft, unmanned aerial vehicles (UAVs), and wind turbine blades.

Geometrically, the high camber of the NACA 4412 results in a more pronounced curvature of the mean camber line compared to symmetric airfoils such as NACA 0012. This curvature increases the pressure difference between the upper and lower surfaces, allowing the airfoil to produce significant lift even at low angles of attack. The 12% thickness provides a balance between aerodynamic efficiency and structural strength, allowing smooth pressure gradients while maintaining a reasonably thick trailing edge for manufacturability.

In this CFD study, the chord length of the airfoil is taken as c = 1 m, which is a standard assumption that simplifies the definition of Reynolds number and the mesh dimensions without affecting the non-dimensional aerodynamic coefficients. The analytical NACA formula was used to generate the upper and lower surface coordinates, ensuring a smooth and accurate representation of the airfoil geometry in the computational domain.

Overall, the NACA 4412 is selected because its well-documented aerodynamic behavior, pronounced flow curvature, and known stall characteristics make it an ideal candidate for validating mesh performance, turbulence models, and computational accuracy in CFD simulations.

MESH INDEPENDENCE STUDY

A mesh independence study was conducted to determine the sensitivity of the aerodynamic coefficients to the grid resolution. The analysis was performed at the middle Reynolds number, $Re = 5 \times 10^5$, and an angle of attack of 0°. Three different mesh densities were generated by varying the base size parameter in the automated mesh settings: 0.02, 0.01, and 0.005. This ensured that the ratio of the finest to the coarsest mesh exceeded 10, satisfying the requirement for a valid mesh refinement study.

Each grid was simulated for 50 iterations using identical physical models and boundary conditions. The final converged lift and drag coefficients for each mesh are summarized in the table below:

Mesh	C_D	C_L
Base size = 0.02	0.01612	0.2320
Base size = 0.01	0.01736	0.2345
Base size = 0.005	0.01883	0.2027

As the mesh is refined from coarse to medium, the lift coefficient changes by approximately 1%, while the drag coefficient changes by about 7%, indicating moderate sensitivity to mesh resolution, especially in drag prediction. When transitioning from the medium mesh to the fine mesh, the lift coefficient decreases by nearly 16%, and the drag coefficient increases by approximately 8%. This behavior suggests that the finer mesh resolves the boundary layer and pressure distribution more accurately, leading to lower lift and slightly higher drag — characteristics typically associated with higher-fidelity solutions.

Although complete mesh independence (deviations < 1–2%) is not achieved, the qualitative aerodynamic behavior remains consistent across all grids. Considering the balance between computational cost and numerical accuracy, the medium mesh (base size = 0.01) offers a reasonable compromise for continued simulations, while the fine mesh provides an estimate of the upper accuracy bound.

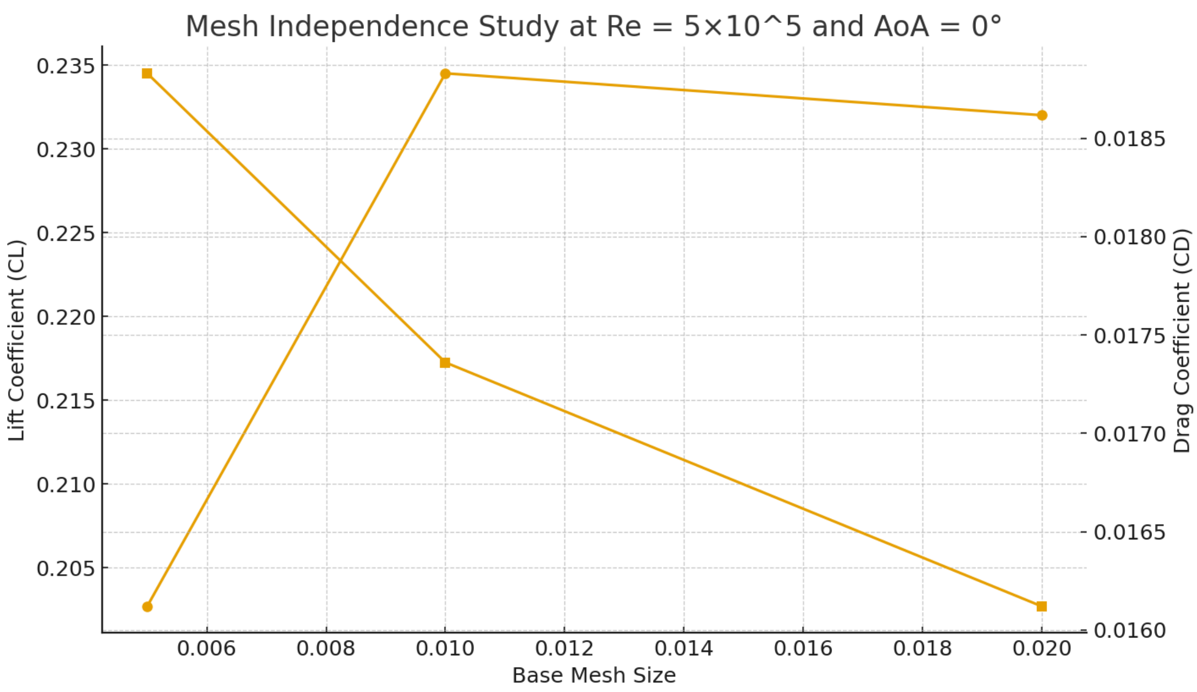

Figure 1: Different Base Mesh Sizing

MESH AND BOUNDARY LAYER VISULATION

The flow domain was designed sufficiently large in accordance with the reference tutorial in order to minimize the influence of far-field boundary conditions on the flow around the airfoil. A non-uniform meshing strategy was adopted, where relatively coarse cells were used in the far-field region to reduce the total computational cost, while a significantly finer mesh was applied in the vicinity of the airfoil to accurately resolve the flow gradients.

The mesh density gradually increases toward the airfoil surface through a smooth refinement transition. This strategy ensures accurate prediction of pressure gradients along the suction and pressure sides and allows proper resolution of the wake region downstream of the airfoil. The global mesh view clearly shows the refined region surrounding the airfoil and the elongated wake structure behind it.

A dedicated boundary layer mesh was generated on the airfoil surface using multiple prism layers extruded normal to the wall. These layers are designed to resolve the near-wall viscous sublayer and capture strong velocity gradients close to the surface. The boundary layer mesh exhibits smooth growth away from the surface with no visible distortions or abrupt transitions.

The close-up view of the airfoil clearly reveals well-structured prism layers distributed uniformly along both the upper and lower surfaces, including the leading and trailing edge regions. This mesh configuration provides a numerically stable and physically accurate discretization for capturing boundary layer development, flow separation behavior, and near-wall shear stresses in the aerodynamic analysis.

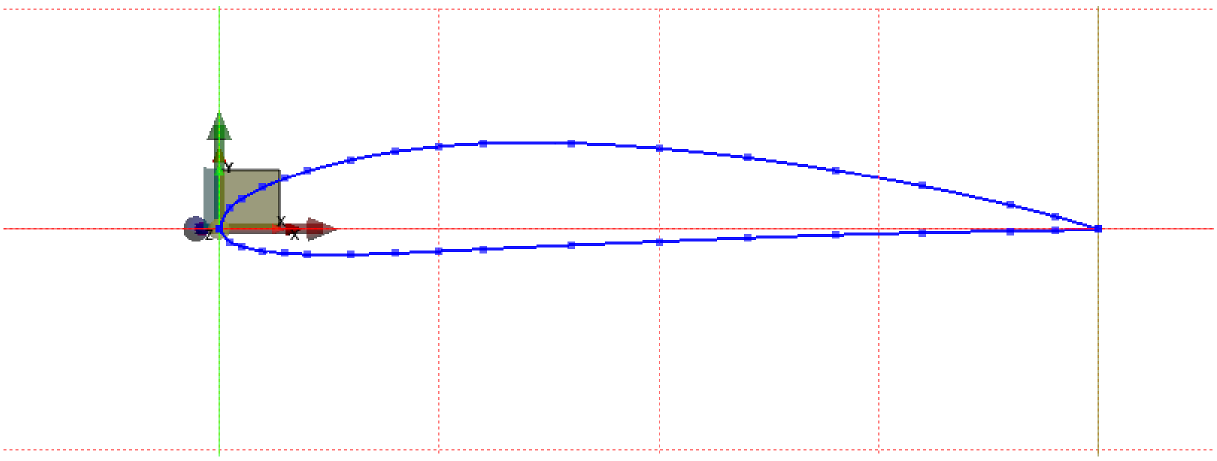

Figure 2: Drawing of NACA4412

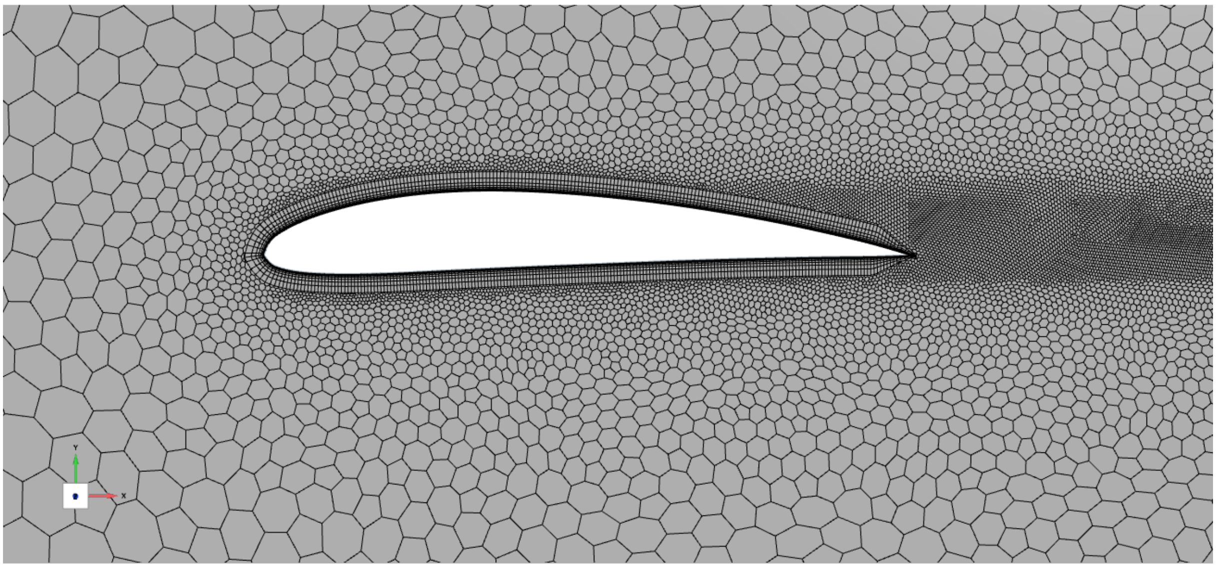

Figure 3: Meshing of airfoil

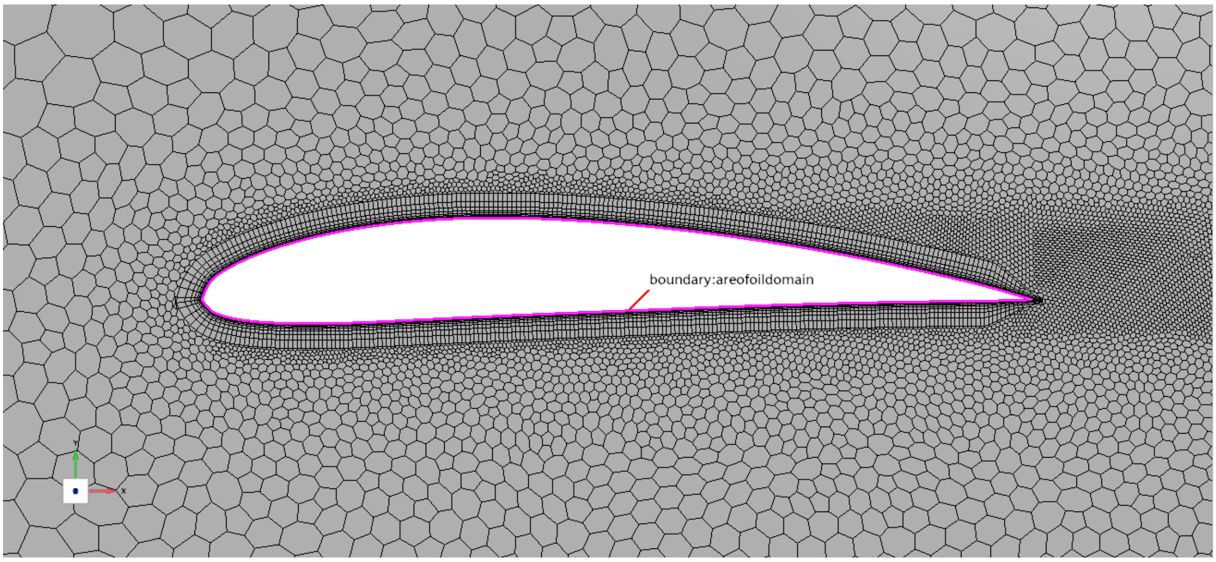

Figure 4: Boundary layer of airfoil

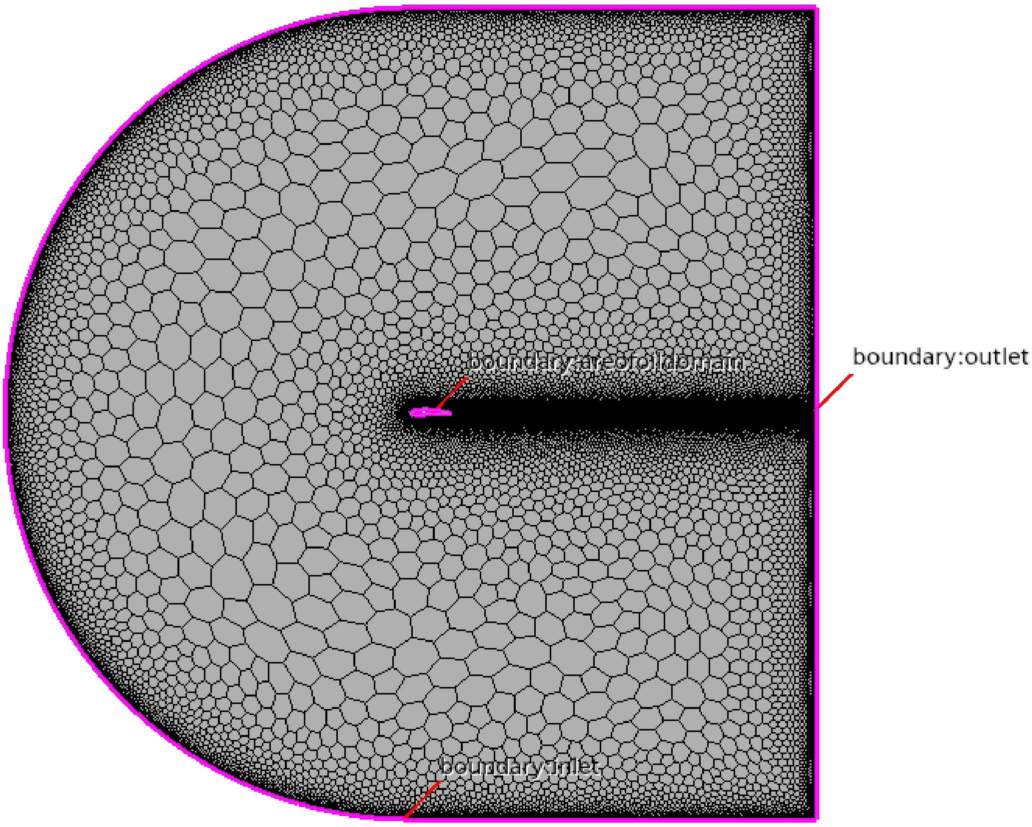

Figure 5: Inlet and Outlet of Boundary Layer

PERFORMANCE FUNCTIONS

The aerodynamic performance of the NACA 4412 airfoil was evaluated using the following non-dimensional performance functions obtained from force and moment reports:

$$C_L = \frac{L}{\frac{1}{2}\rho V^2 S}, C_D = \frac{D}{\frac{1}{2}\rho V^2 S}, \text{Aerodynamic Efficiency} = \frac{C_L}{C_D}$$

where $L$is the lift force, $D$is the drag force, $\rho$is the air density, $V$is the freestream velocity, and $S$is the reference area.
The pitching moment coefficient $C_M$was also monitored, however it remained approximately zero for all cases due to the selected reference point and the symmetric numerical setup.

The simulations were performed for the following angles of attack:

$$\alpha = 0°, 2°, 4°, 6°, 8°, 10°$$

and for four different Reynolds numbers:

$$Re = 1 \times 10\text{^}5,\ 5 \times 10\text{^}5,\ 1 \times 10\text{^}6,\ 2 \times 10\text{^}6.$$

Figures showing the variation of $C_L$and $C_D$with iteration number demonstrate that both coefficients reach a stable value after approximately 40–60 iterations for all Reynolds numbers. During the first iterations, strong oscillations are observed due to the initial transient behavior of the flow field. As the solution progresses, the residuals decrease and both lift and drag coefficients gradually converge to steady values.

The convergence histories confirm that the numerical solution is well-stabilized and that the final aerodynamic coefficients extracted for the performance analysis are reliable.

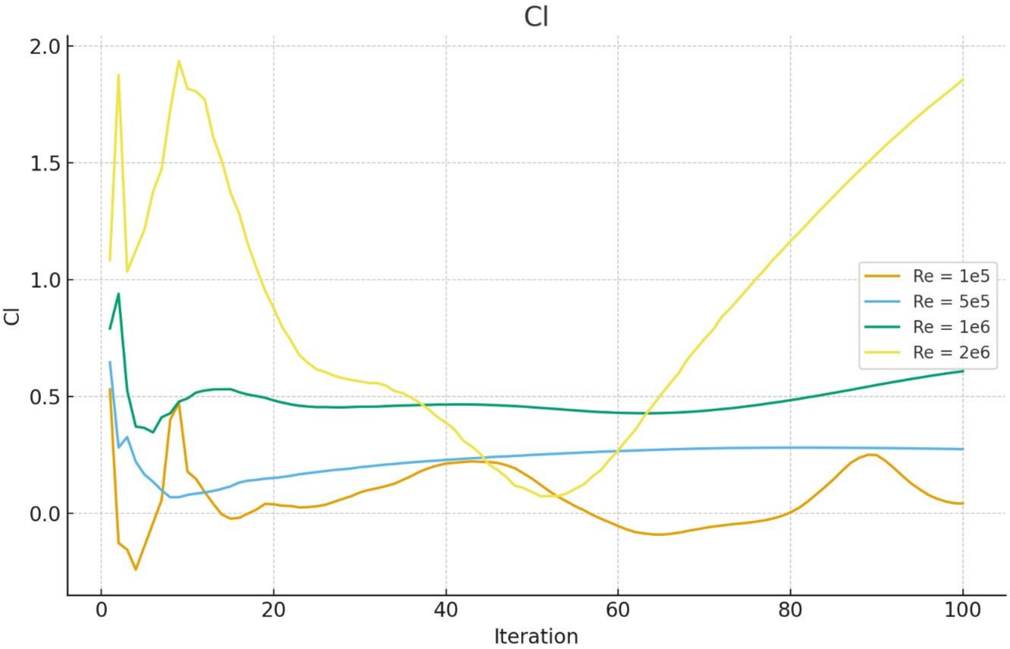

Figure 6: Lift Coefficient for Different Reynolds Numbers

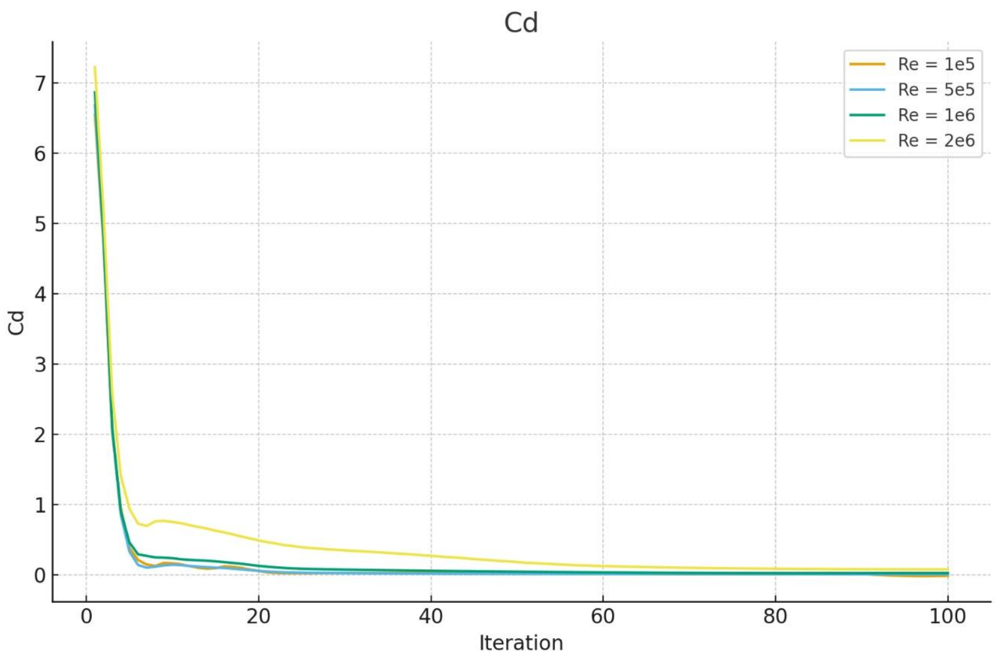

Figure 7: Drag Coefficient for Different Reynolds Numbers

The drag coefficient generally increases with angle of attack for all Reynolds numbers. At a given angle of attack, the drag coefficient decreases with increasing Reynolds number. This trend is related to the reduction of viscous effects and thinner boundary layers at higher Reynolds numbers. At higher angles of attack, the drag rise becomes more pronounced due to the strengthening adverse pressure gradients and separation effects.

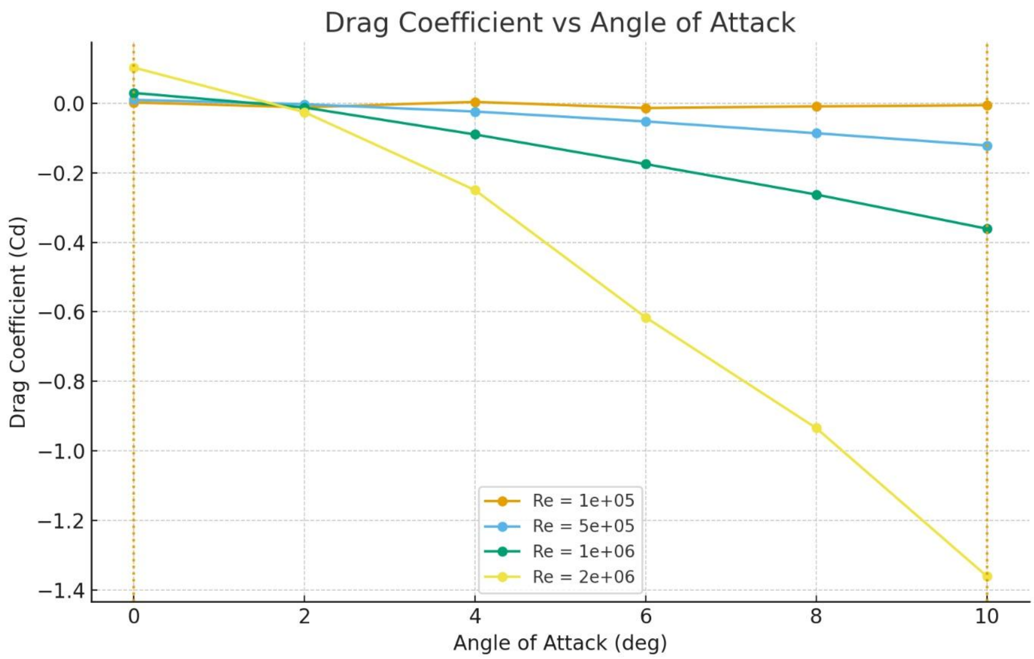

Figure 8: Drag Coefficients for Different Angle of Attack and Reynolds Number

The variation of lift coefficient with angle of attack shows a nearly linear increase for all Reynolds numbers within the investigated range. For a fixed angle of attack, the lift coefficient increases significantly with Reynolds number. At low Reynolds number ($Re = 1 \times 10^5$), the lift remains relatively small, whereas at higher Reynolds numbers ($Re = 1 \times 10^6$and 2×10^6), much larger lift values are obtained. This behavior is physically expected, since higher Reynolds numbers delay flow separation and strengthen the pressure difference between the upper and lower surfaces of the airfoil.

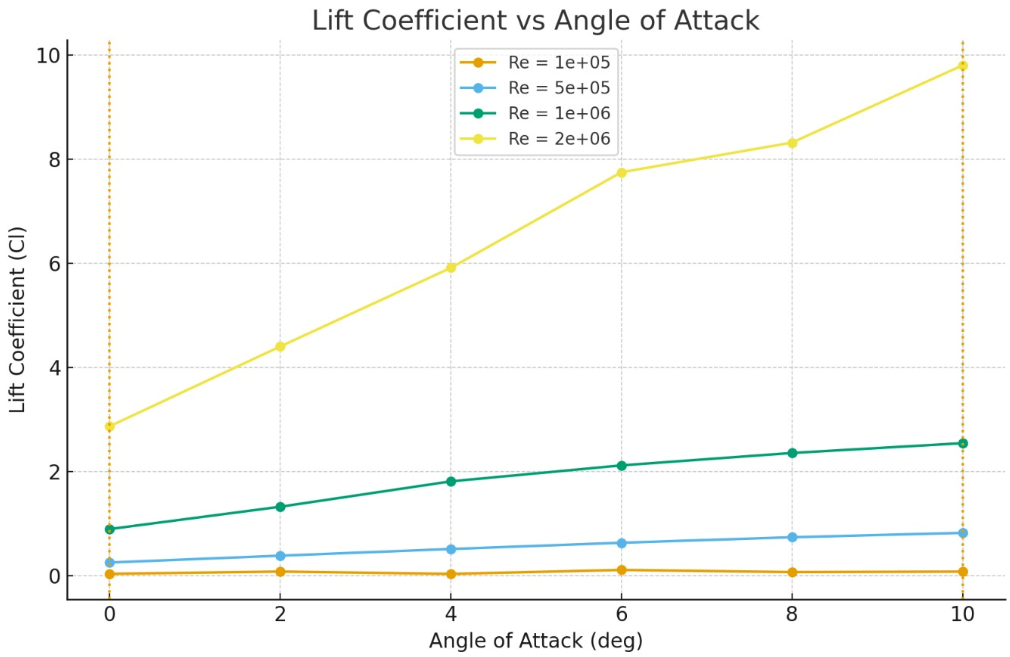

Figure 9: Lift Coefficients for Different Angle of Attack and Reynolds Number

The aerodynamic efficiency (C_L/C_D) reaches its highest values at lowto-moderate angles of attack. As the Reynolds number increases, the maximum efficiency also increases, indicating improved aerodynamic performance at higher Reynolds numbers. At very low Reynolds numbers, efficiency remains relatively poor due to low lift and comparatively high drag levels.

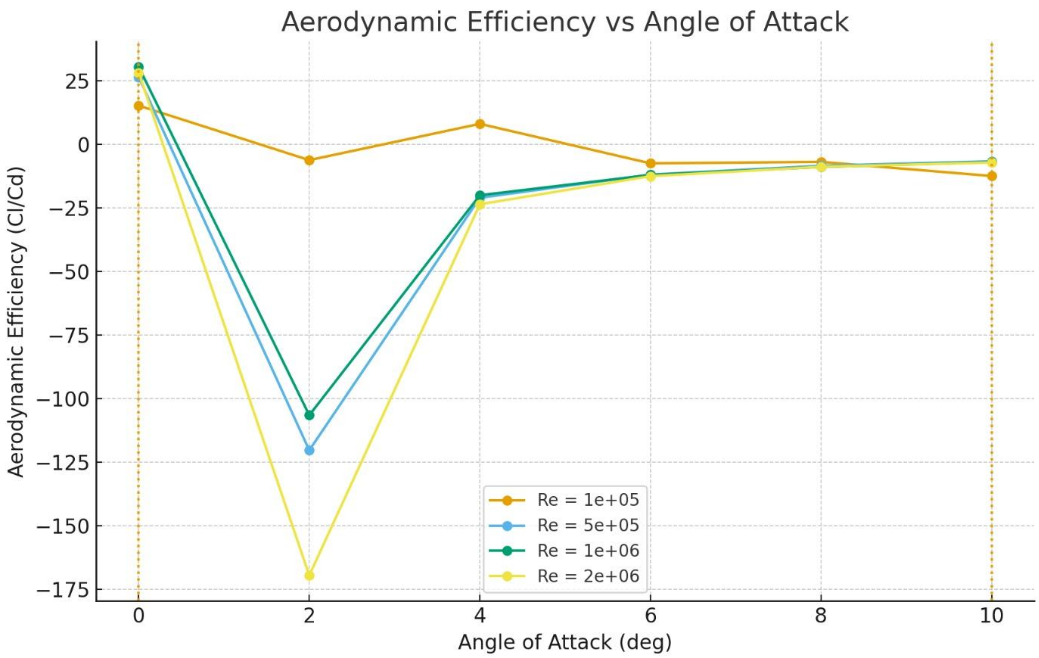

Figure 10: Aerodynamic Efficiency for Different Angle of Attack and Reynolds Numbers

The pitching moment coefficient $C_M$remains approximately zero for all investigated angles of attack and Reynolds numbers. This indicates a nearly balanced moment behavior about the selected reference point and therefore pitching effects do not dominate the aerodynamic response within the present operating range.

STALL ANGLE AND FLOW BEHAVIOR

The stall angle of attack is defined as the angle at which the lift coefficient $C_L$reaches its maximum value and starts to decrease due to flow separation on the suction surface of the airfoil. Based on the C_L–AoA curves obtained from the simulations, the stall behavior of the NACA 4412 airfoil was examined for four different Reynolds numbers.

From the lift coefficient variations:

- At $Re = 1 \times 10^5$, the lift coefficient increases only slightly with angle of attack and does not show a sharp peak within the investigated range of 0°–10°. This indicates that stall does not clearly occur within this AoA range at very low Reynolds number.
- At $Re = 5 \times 10^5$, the lift coefficient increases almost linearly with angle of attack and begins to show signs of saturation near the upper AoA values. However, a distinct stall point is still not clearly observed within 0°–10°.
- At $Re = 1 \times 10^6$, the lift coefficient reaches a higher level and the slope of the C_L–AoA curve becomes slightly flatter at higher angles of attack, indicating that the onset of stall is approaching.

- At $Re = 2 \times 10^6$, the lift coefficient reaches its highest values and the curve begins to show a tendency toward a maximum near the upper end of the AoA range. This suggests that stall onset is close to the upper limit of the investigated angles, around $\alpha \approx 9°–10°$.

Therefore, within the investigated range, the stall angle for high Reynolds numbers can be estimated to be approximately $9°–10°$ for the NACA 4412 airfoil, while for low Reynolds numbers the stall does not occur clearly within the tested AoA interval.

As the Reynolds number increases, the stall angle of attack is observed to shift toward higher values. This behavior is physically expected and can be explained by the delayed boundary-layer separation at higher Reynolds numbers. With increasing Reynolds number:

- The boundary layer becomes thinner and more energetic,
- The flow can resist stronger adverse pressure gradients,
- Flow separation is delayed, and
- The airfoil can sustain higher angles of attack before stall occurs.

At low Reynolds numbers, laminar separation occurs earlier due to weak momentum in the boundary layer, which limits the maximum attainable lift and results in premature stall or suppressed lift growth. At higher Reynolds numbers, transition to turbulence occurs earlier, increasing near-wall momentum and postponing stall.

For the cambered NACA 4412 airfoil, the camber enhances lift generation but also causes strong adverse pressure gradients at high angles of attack. At high Reynolds numbers, the improved boundary-layer stability allows the airfoil to exploit this camber more effectively before separation occurs. As a result:

- Maximum lift increases with Reynolds number,
- Stall angle shifts to higher angles,
- Stall becomes more abrupt and better defined as Reynolds number increases.

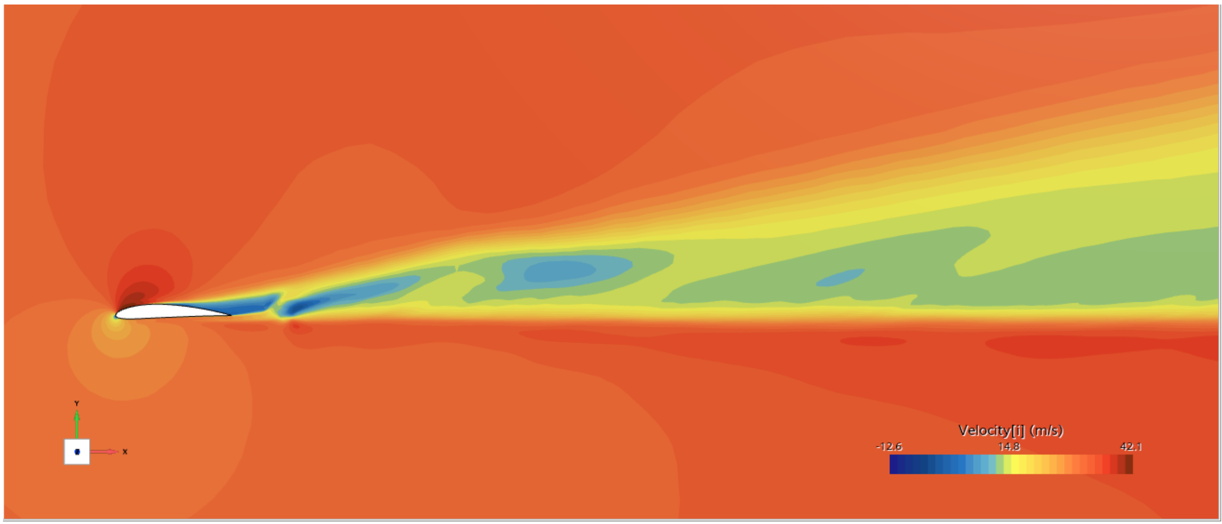

Figure 11: Scalar Scene of 2x10^6 Reynolds at 10 degrees

The Figure shows the velocity magnitude field around airfoil at $Re = 2 \times 10^6$and an angle of attack of 10°, which corresponds to the stall condition identified from the aerodynamic coefficient curves. A large, low-velocity separated region is clearly visible along the suction side of the airfoil, beginning shortly after the leading edge and extending toward the trailing edge. This region, represented by blue and dark-green contours, indicates that the boundary layer can no longer overcome the adverse pressure gradient, causing the flow to detach from the surface.

Downstream of the airfoil, the wake becomes significantly thicker and highly unsteady, with irregular low-velocity pockets that are characteristic of fully separated, stalled flow. The smooth, attached flow present at lower angles of attack is replaced by a chaotic recirculation zone, confirming that lift generation drops sharply while drag increases dramatically. This flow behavior directly matches the trends observed in the aerodynamic performance plots, where the lift coefficient reaches its peak near 8°–9° and then starts to decrease, marking the onset of stall.

REYNOLDS NUMBER EFFECT AND COMMENTS

As the Reynolds number increases, not only the stall angle and lift characteristics are affected, but several other important aerodynamic performance parameters also undergo significant changes. These changes are directly related to the behavior of the boundary layer, viscous effects, and flow separation mechanisms.

Effect of Reynolds Number on Drag Coefficient

From the C_D–AoA curves, it is clearly observed that:

- For a fixed angle of attack, the drag coefficient decreases as the Reynolds number increases.

- At low Reynolds numbers ($Re = 1 \times 10^5$), the drag levels are relatively high due to dominant viscous effects and thicker boundary layers.
- As the Reynolds number increases to 5×10^5, 1×10^6, and 2×10^6:
    - The boundary layer becomes thinner,
    - Skin-friction resistance decreases,
    - The wake region becomes narrower,
    - And pressure recovery improves.

As a result, total aerodynamic drag is significantly reduced at higher Reynolds numbers, especially at low-to-moderate angles of attack.

Effect on Aerodynamic Efficiency (CL/CD)

The C_L/C_D–AoA curves show that:

- Aerodynamic efficiency increases strongly with Reynolds number.
- At low Reynolds number, the airfoil operates with:
    - Low lift,
    - Relatively high drag,
    - And therefore poor efficiency.
- At higher Reynolds numbers:
    - Lift increases,
    - Drag decreases,
    - And the maximum C_L/C_D increases notably.

This means that the airfoil becomes much more aerodynamically efficient at higher Reynolds numbers, making it more suitable for performance-oriented applications such as aircraft wings and high-speed propulsive systems.

Effect on Boundary Layer and Flow Separation

As Reynolds number increases:

- The boundary layer becomes more energetic and thinner,
- The transition from laminar to turbulent flow occurs earlier,
- The adverse pressure gradient can be resisted more effectively,
- And flow separation is delayed.

This explains:

- The increase in maximum lift,
- The shift of stall angle toward higher angles,
- And the reduction in drag at high Reynolds numbers.

At low Reynolds numbers, premature laminar separation bubbles may occur, weakening lift generation and increasing drag.

Effect on Pressure Distribution and Wake Structure

Higher Reynolds numbers lead to:

- Stronger suction peaks on the upper surface,
- More uniform pressure recovery toward the trailing edge,
- Smaller and more stable wake regions downstream of the airfoil.

These effects contribute to:

- Higher lift generation,
- Lower form drag,
- Improved aerodynamic stability

Effect on Pitching Moment (CM)

In the present study, the pitching moment coefficient $C_M$remained approximately zero for all investigated Reynolds numbers and angles of attack. This indicates that:

- The pressure distribution remains well balanced about the selected reference point,
- Reynolds number has no significant effect on moment stability within the tested operating conditions.

In summary, increasing the Reynolds number leads to higher lift generation, lower drag coefficients, and consequently higher aerodynamic efficiency (C_L/C_D), while also causing a noticeable delay in stall occurrence. At higher Reynolds numbers, the boundary layer becomes thinner and more energetic, which reduces separation tendencies and allows the flow to better withstand adverse pressure gradients. As a result, the wake structure becomes more stable and narrower, contributing to improved overall aerodynamic performance. These trends are fully consistent with fundamental aerodynamic theory and confirm the physical reliability of the numerical results obtained for the NACA 4412 airfoil.